nature biotechnology

Engineering of a monomeric green-to-red photoactivatable fluorescent protein induced by blue light

Nadya G Gurskaya[1], Vladislav V Verkhusha[2], Alexander S Shcheglov[1], Dmitry B Staroverov[3], Tatyana V Chepurnykh[3], Arkady F Fradkov[1], Sergey Lukyanov[1] & Konstantin A Lukyanov[1]

Green fluorescent protein (GFP) and GFP-like proteins represent invaluable genetically encoded fluorescent probes[1,2]. In the last few years a new class of photoactivatable fluorescent proteins (PAFPs) capable of pronounced light-induced spectral changes have been developed[3]. Except for tetrameric KFP1 (ref. 4), all known PAFPs, including PA-GFP[5], Kaede[6], EosFP[7], PS-CFP[8], Dronpa[9], PA-mRFP1[10] and KikGR[11] require light in the UV-violet spectral region for activation through one-photon excitation—such light can be phototoxic to some biological systems[12]. Here, we report a monomeric PAFP, Dendra, derived from octocoral *Dendronephthya sp.* and capable of 1,000- to 4,500-fold photoconversion from green to red fluorescent states in response to either visible blue or UV-violet light. Dendra represents the first PAFP, which is simultaneously monomeric, efficiently matures at 37 °C, demonstrates high photostability of the activated state, and can be photoactivated by a common, marginally phototoxic, 488-nm laser line. We demonstrate the suitability of Dendra for protein labeling and tracking to quantitatively study dynamics of fibrillarin and vimentin in mammalian cells.

Several years ago we cloned green fluorescent protein dendGFP from octocoral *Dendronephthya sp.* along with other fluorescent proteins[13]. dendGFP carries a histidine residue in the chromophore-forming triad His62-Tyr63-Gly64 (**Supplementary Fig. 1** online). Histidine in that position is characteristic for a group of green-to-red Kaede-like PAFPs such as Kaede from *Trachyphyllia geoffroyi*[9,14], EosFP from *Lobophyllia hemprichii*[7] and engineered KikGR[11]. Indeed, we found that dendGFP can be readily converted into a red fluorescent state by irradiation in the UV-violet spectral region. It is interesting to note that *T. geoffroyi* and *Dendronephthya sp.* represent different Anthozoa subclasses (Zoantharia and Alcyonaria, respectively). Thus, the green-to-red PAFPs from these species provide a striking example of convergent evolution at the molecular level.

To make dendGFP suitable for protein labeling we generated a monomeric variant, named Dendra (from *Dendronephthya sp.*, red activatable), using mutagenesis strategy suggested for monomerization of green fluorescent protein Azami-Green[15] (see **Supplementary Data**, **Supplementary Figs. 1–3** and **Supplementary Table 1** online for details on Dendra mutagenesis, oligomeric and spectral properties). In contrast to a recently developed monomeric version of EosFP, called mEosFP[7,16], Dendra completely matures at 37 °C in both bacterial and

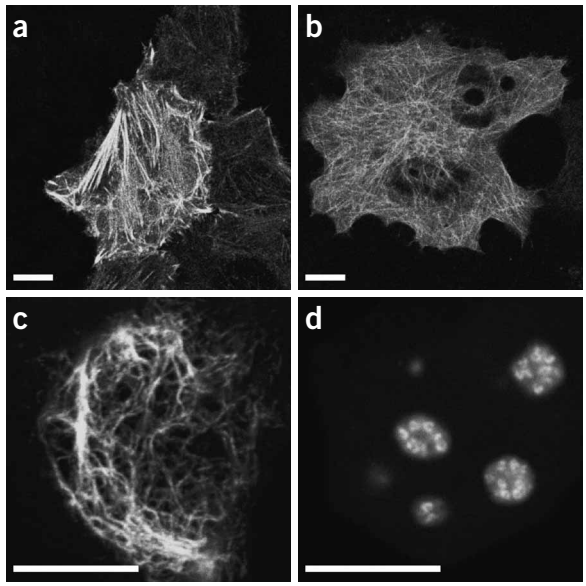

Figure 1 Labeling of intracellular oligomerizing proteins with Dendra. Confocal images of HeLa cells transiently expressing Dendra fused with (**a**) β-actin, (**b**) α-tubulin, (**c**) vimentin or (**d**) fibrillarin are shown. For corresponding EGFP-tagged proteins, we observed similar signal distribution (not shown). Bars, 10 μm.

[1]Institute of Bioorganic Chemistry, Russian Academy of Sciences, Miklukho-Maklaya 16/10, Moscow 117997, Russia. [2]Department of Anatomy and Structural Biology, Albert Einstein College of Medicine, Bronx, New York 10461, USA. [3]Evrogen JSC, Miklukho-Maklaya 16/10, Moscow 117997, Russia. Correspondence should be addressed to K.A.L. (kluk@ibch.ru).

Received 22 September 2005; accepted 13 December 2005; published online 19 March 2006; doi:10.1038/nbt1191

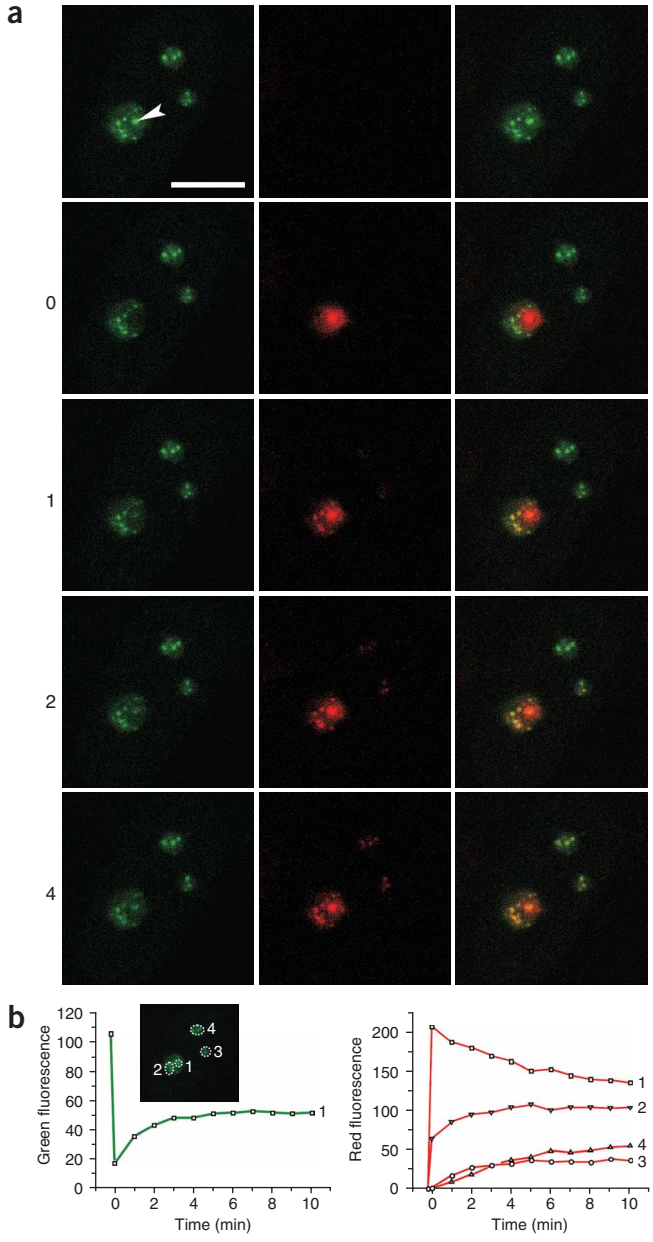

Figure 2 Tracking Dendra-fibrillarin in HeLa cells. (**a**) Time-lapse series of confocal images of a single cell before (upper row) and after Dendra photoactivation at the point designated by the arrow. Left column, green signal; middle column, red signal; right column, overlay. Numbers on the left indicate time after photoactivation in minutes. Bar, 10 μm. (**b**) Graphic representation of green (left) and red (right) signal intensities in selected regions 1–4 shown in the inset. Region 1 represents activation point; region 2, a nonactivated portion of the activated nucleolus; regions 3 and 4, adjacent nucleoli.

mammalian cells. Bacterial colonies expressing Dendra can be irreversibly converted from green (excitation and emission maxima at 486 and 505 nm, respectively) to red (excitation and emission maxima at 558 and 575 nm, respectively) fluorescent states by irradiation with a 405-nm light using a fluorescent stereomicroscope. For purified Dendra, we achieved a 350-fold increase of red fluorescence and a fivefold decrease of green fluorescence resulting in a 1,400-fold contrast between the ground and activated states.

Green and red fluorescent states of Dendra are characterized by molar extinction coefficients of 21,000 and 20,000 $M^{-1}cm^{-1}$ and fluorescence quantum yields of 0.72 and 0.70, respectively (**Supplementary Table 1** online). Fluorescence brightness of purified Dendra is lower compared to the wild-type dendGFP. However, bacterial colonies expressing Dendra appeared substantially brighter than those with dendGFP indicating either more complete maturation or more efficient folding of Dendra.

Photostability of photoconverted Dendra was evaluated in comparison to commonly used Anthozoa red fluorescent protein DsRed[17]. Individual bacterial cells expressing either Dendra (activated through FITC filter) or DsRed were bleached by 543-nm laser line in confocal microscope. Under identical irradiation conditions DsRed reached 50% bleaching 3.3 times faster than Dendra (**Supplementary Table 1** online). Thus Dendra possesses substantially higher photostability compared to DsRed, which is particularly useful for long-term protein tracking applications.

Evaluating Dendra expression in mammalian cells we found that intense blue light also converts the protein into a red fluorescent state. Several-seconds irradiation through an FITC filter (450–490 nm, 0.5–0.7 W/cm^2) resulted in the appearance of bright red fluorescence in Dendra-expressing cells. At the same time, exposure to low-intensity blue light (<50 mW/cm^2) for the same time interval did not result in detectable photoconversion. We further studied dependence of Dendra photoconversion on the intensity of activating blue light using confocal microscopy of purified Dendra protein immobilized on TALON beads. Red fluorescence increase was evaluated after scanning with 488-nm laser of different intensities. We observed a nonlinear, sigmoidal dependence (**Supplementary Fig. 3b** online) indicating that Dendra requires sequential absorption of two photons to be converted into the red state. Even prolonged scanning with 488-nm light density below 50 mW/cm^2 resulted in zero red fluorescence increase. This behavior makes it easy to select distinct blue light intensities appropriate for (i) visualization of green fluorescence without photoconversion and (ii) local Dendra green-to-red photoconversion. Similar activation behavior was also observed for wild-type dendGFP. Since no other Kaede-like PAFPs exhibited green-to-red irreversible conversion in response to visible blue light, dendGFP and its mutants represent a new group of PAFPs.

To test Dendra's ability to label target proteins, we constructed plasmids for expression of Dendra in fusion with human β-actin, α-tubulin, vimentin and fibrillarin. In transiently transfected HeLa cells we observed expected patterns of signal distribution (**Fig. 1**) similar to those of the corresponding enhanced (E)GFP-tagged proteins[18–21] (not shown) indicating the monomeric state of Dendra in mammalian cells. All fusion proteins tested underwent pronounced photoconversion by an intense 488-nm laser line of confocal microscope (100–200 ms continuous irradiation with 200 W/cm^2 or 5–8 scans at a selected cell region with about 1.5 W/cm^2) giving exactly the same distribution of green signal before and red signal after the conversion. The decrease in green fluorescence observed in living cells was 10- to 15-fold and the increase in red fluorescence was 150- to 300-fold, which resulted in 1,500- to 4,500-fold photoconversion contrast.

To demonstrate the applicability of Dendra for protein tracking, we first monitored the movement of Dendra-fibrillarin fusion protein within interphase nuclei of HeLa cells (**Fig. 2**). Scanning with a low-level (3 mW/cm^2) 488-nm laser line allowed visualization of green signal in cells containing Dendra-fibrillarin in nucleoli. Primary visualization did not result in detectable photoconversion of Dendra

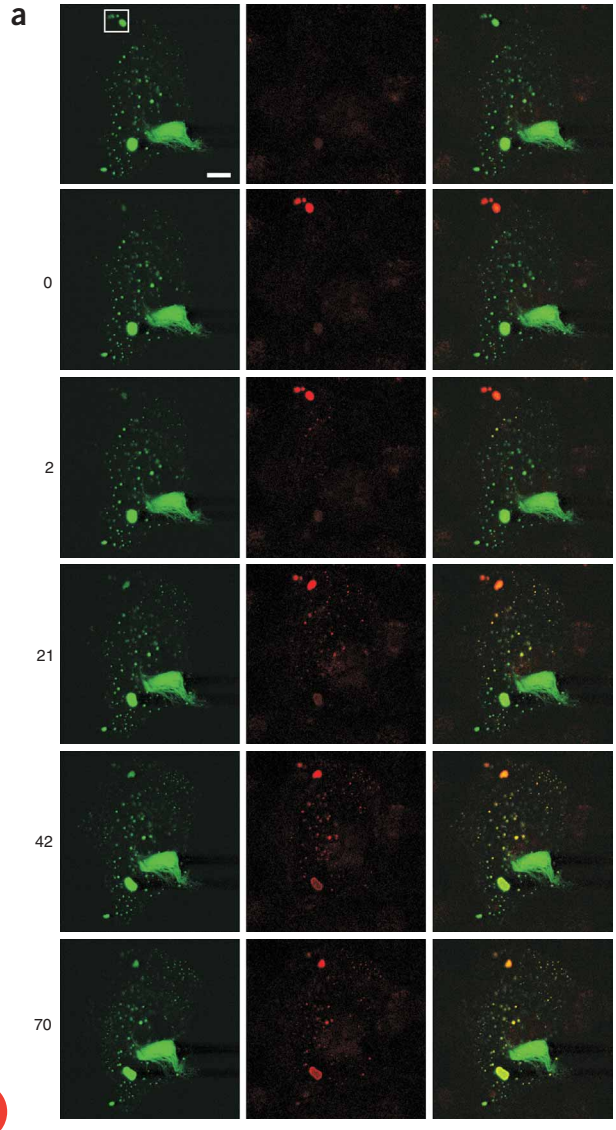

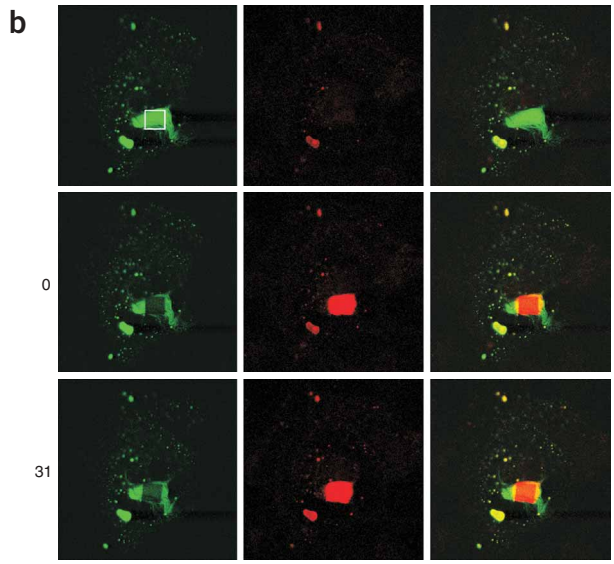

Figure 3 Tracking Dendra-vimentin in a HeLa cell containing vimentin in both dots and filaments. Left column, green signal; middle column, red signal; right column, overlay. Numbers on the left indicate time after photoactivation in minutes. Bar, 10 μm. (**a**) Photoactivation of Dendra-vimentin in selected dots (white square) and its following tracking. (**b**) After time-lapse series shown in **a**, the activated Dendra red signal was partially bleached (upper row). Then, an area within filaments (white square) was photoactivated. Note an effective exchange of vimentin between the dots and its low mobility in the filaments.

into the red state. Local green-to-red conversion was achieved by 200-ms irradiation of a point within one nucleolus with intense 488-nm laser line (200 W/cm^2). After that, a time-lapse series of images demonstrated migration of the red signal first within the activated nucleolus and then to adjacent nucleoli (**Fig. 2** and **Supplementary Video 1** online).

Mobile and immobile Dendra-fibrillarin fractions can be estimated from green signal recovery in the region of photoconversion (also, these values can be derived from comparison of final red fluorescence intensities in activated and nonactivated nucleoli with correction to the brightness of these points before photoconversion in the green channel). Direct visualization of Dendra-fibrillarin red signal migration from the activation point allows estimation of the rate of the fusion protein (i) migration within nucleolus, (ii) dissociation from the activated nucleolus to nucleoplasm, (iii) migration in the nucleoplasm and (iv) accumulation in adjacent nucleoli. We found that individual HeLa cells ($n = 16$) demonstrated substantial differences in Dendra-fibrillarin motility. From cell to cell, immobile fractions varied from 35–75%, and half-times of Dendra-fibrillarin migration from activated to nonactivated nucleoli varied from 10–200 s (that corresponds to efficient diffusion coefficients of 2.7–0.07 μm^2 s^{-1}). For example, the recovery curve of the green signal in the activation point (**Fig. 2b**, region 1) indicated a 46% immobile fraction. The red signal increased with a half-time of 6, 60 and 130 s in regions 2, 3 and 4, respectively (**Fig. 2b**). Considering the different distances between activation region 1 and regions 2, 3 and 4 (diffusion areas 13, 140 and 220 μm^2, respectively), we estimated the efficient diffusion coefficient of Dendra-fibrillarin to be 0.50 ± 0.08 μm^2 s^{-1} in this cell. The majority of cells demonstrated an ~50% immobile fraction and efficient diffusion coefficient of about 0.3 μm^2 s^{-1}. Migration of the activated red signal in nucleoplasm was always fast (<10 s for signal migration throughout the nucleus). Similar values of the immobile fraction and the diffusion coefficient of Dendra-fibrillarin was observed in human kidney 293T-derived Phoenix Eco cell line (not shown).

Moreover, a substantial decrease in the Dendra-fibrillarin green signal allowed a simultaneous conventional fluorescence recovery after photobleaching (FRAP) analysis to be done. For instance, an ~60-s half-time for green fluorescence recovery was observed for a 3-μm^2 photoconverted area (**Fig. 2**). Indeed, kinetics parameters of the green fluorescence recovery in the photoconverted region were close to those described earlier with EGFP-fibrillarin fusion[21].

Next we studied the intracellular dynamics of Dendra fused to vimentin, a protein of intermediate cytoskeletal filaments. Consistent with previous data[22,23], we observed two types of vimentin patterns in HeLa cells. The majority of cells contained complex networks of filamentous vimentin (**Fig. 1c**). In other cells, vimentin was found mostly in dots of different size with few filaments present. The typical experiment on Dendra-vimentin dynamics in cells of the second type is shown in **Figure 3**. Scanning a small cell region with a high-intensity

488-nm laser (1.4 W/cm^2), we photoconverted Dendra in some of the dots (**Fig. 3a** and **Supplementary Video 2** online). Then, an effective exchange of red signal between the activated and nonactivated vimentin dots occurred. Naturally, the nearest dots accumulated red signal faster than the distant ones. Considering half-time of red fluorescence growth in nonactivated dots and their distances from activated dots, we estimated the efficient diffusion coefficient to be 0.35 μm^2 s^{-1}. The immobile fraction varied from 75% for large (about 6 μm^2) dots to 20% for small (about 0.5 μm^2) dots. Notably, the activated Dendra-vimentin did not enter into filaments. Next, Dendra-vimentin was activated within the filamentous structure of the same cell (**Fig. 3b**). In this case, during 0.5 h we detected only extremely slow migration of Dendra-vimentin from or toward the activated filamentous zone. In particular, green fluorescence after 12-fold bleaching within the activated area increased only 1.7-fold (less than 5% of the mobile fraction). Red fluorescence in the vimentin dots increased about 1.3-fold. No change in either green or red fluorescence was detected in the nonactivated filamentous vimentin areas.

Our experiments demonstrate drastic differences in the mobility of vimentin molecules in punctate and filamentous structures within the same cell. Also, the pools of punctate and filamentous vimentin were shown to be generally separate. It has been shown that punctate vimentin structures contain mostly phosphorylated vimentin[22]. The observed vimentin dynamics allows us to speculate that phosphorylation greatly affects not only the localization patterns but also the mobile properties of vimentin. Phosphorylated punctate vimentin represents a highly mobile protein pool, whereas nonphosphorylated vimentin in filaments has little mobility.

The structural basis for Dendra sensitivity to blue light still remains unclear. It has been demonstrated for Kaede-like PAFPs that blue light does not convert them into the red fluorescent state. Only the neutral (protonated) form of GFP-like chromophore, which absorbs at 380–420 nm, was converted into the red (anionic) chromophore in these PAFPs[6,7,11,14]. At the same time, anionic (deprotonated) GFP-like chromophore, which absorbs at ~480 nm, was completely insensitive to blue light irradiation. We also found that many red-shifted fluorescent and chromoproteins mature through the neutral GFP-like chromophore whereas the anionic chromophore is a side product, which never converts into the red chromophore[24]. One possible explanation for Dendra peculiarity is its high pK_a, which might facilitate fast protonation of the excited anionic green chromophore. As a result the excited neutral chromophore capable of chemical transformation into the red chromophore might appear. However, recently developed KikGR with high pK_a (7.8) demonstrated no convertibility by blue light[11]. Therefore Dendra possesses some distinct structural features ensuring photoconversion in response to blue light. Comparison of interior amino acids shows only a few differences between dendGFP/Dendra and Kaede, EosFP and KikGR (**Supplementary Fig. 1** online). Among the differences one can note residue 116, which is glutamine in Dendra but asparagine in other Kaede-like proteins. Our analysis of EosFP crystal structure[25] shows that the longer glutamine side-chain at this position can contact the protein backbone near the chromophore-forming His62 residue. Possibly, this contact can facilitate backbone breakage and red chromophore formation in response to low-energy blue light (as compared to UV light). Further studies are required to clarify the mechanism of Dendra photoconversion.

Comparison of activation conditions for different PAFPs (refs. 4–12, **Supplementary Table 2** online) showed that Dendra possesses a clear advantage in respect to potential harmfulness of activating light. Indeed, Dendra requires longer-wavelength blue light of similar or even lower intensity compared to UV-violet light, which was used to activate PA-GFP, PS-CFP and Kaede-like proteins in cells. It was demonstrated that photoconversion of KikGR[11] and EosFPs[16] results in no detectable phototoxicity. At the same time, photoactivation of PA-GFP by 408-nm laser in nuclei led to stopping of cell divisions[12]. Two-photon activation solved this problem to some extent, but only low-contrast PA-GFP activation in viable nuclei was achieved[12]. Aside from easily detectable cell death, UV irradiation can induce hidden changes in cell biochemistry. For instance, recent studies demonstrated that irradiation of human keratinocytes by 365-nm light (10–20 J/cm^2 dose, which is comparable to light doses used for PAFPs photoconversion; see **Supplementary Table 2** online) resulted in activation of extracellular signal-regulated kinase (ERK) and Ras and an increase in intracellular calcium level[26], as well as in disintegration of connexin 43-formed gap junctions and actin microfilaments[27]. Such changes can affect biological relevance of PAFP tracking results. Finally, an important practical advantage of Dendra is the widespread availability of 488-nm lasers in contrast to the quite rare and expensive UV and multiphoton lasers.

In conclusion, compared to other available PAFPs, Dendra provides a combination of advantageous properties such as the monomeric state suitable for protein labeling, highly contrasting photoconverion with fluorescence at the red spectral region, the low-phototoxic activation with 488-nm light available on common confocal microscopes, the high photostability of the photoconverted state and efficient chromophore maturation at 37 °C in mammalian cells.

METHODS

Mutagenesis and protein characterization. Site-directed mutagenesis was performed by overlap-extension PCR with specific oligonucleotides containing the corresponding target substitutions[28]. Diversity PCR Random Mutagenesis kit (Clontech) was used for error-prone PCR, in conditions optimal for seven mutations per 1,000 bp. For bacterial expression, the full-length coding region was amplified using specific primers and subcloned into the pQE30 (Qiagen). Fluorescent proteins fused to a N-terminal polyhistidine tag were expressed in *Escherichia coli* XL1 Blue strain (Invitrogen). Fluorescent stereomicroscope SZX-12 (Olympus) was used for visual screening of bacterial colonies expressing mutant proteins. Photoconversion of colonies was achieved either by stereomicroscope 405BP10-nm excitation filter (0.6 W/cm^2 for 10–20 s) or by sunlight for several hours.

Proteins were purified using TALON metal-affinity resin (Clontech). Oligomeric state of proteins was analyzed by size-exclusion gel-filtration using AKTAprime chromatograph (Amersham Pharmacia Biotech). Purified protein samples (~1 mg/ml) were loaded onto a Sephadex-100 column (0.7 × 60 cm) and eluted with 50 mM phosphate buffer (pH 7.0) containing 100 mM NaCl. EGFP, HcRed1 and DsRed2 proteins (Clontech) were used as monomer, dimer and tetramer standards, respectively. Absorption and excitation-emission spectra were recorded with Beckman DU520 UV/VIS spectrophotometer and Varian Cary Eclipse fluorescence spectrophotometer. For fluorescence quantum yield determination, the fluorescence of dendGFP and Dendra before and after photoconversion was compared to equally absorbing samples of EGFP (quantum yield 0.6; ref. 29) or DsRed2 (quantum yield 0.55; ref. 30). Molar extinction coefficients were measured as described[8].

Gene construction for expression in mammalian cells. For expression in eukaryotic cells, the PCR-amplified *Age*I-*Xho*I fragment encoding Dendra was inserted in lieu of the EGFP-coding region in the pEGFP-C1 vector (Clontech) resulting in pDendra-C1 plasmid. For construction of α-tubulin and vimentin fusions, we added a linker containing SGDSGVYKT amino acids to the Dendra C terminus resulting in pDendra-elo-C1. For this a PCR-amplified *Age*I-*Xho*I fragment encoding elongated Dendra was swapped with EGFP in pEGFP-C1 vector. *Nhe*I-*Xho*I fragment of elongated Dendra from pDendra-elo-C1 was swapped with EGFP in pEGFP-tubulin vector (Clontech). cDNA encoding human vimentin was obtained from EGFP-vimentin plasmid. This plasmid was

a generous gift from R.D. Goldman. To generate the Dendra-vimentin fusion, we cut out an *Age*I-*Kpn*I fragment encoding elongated Dendra from pDendra-elo-C1 and inserted it into the respective sites of EGFP-vimentin plasmid. To generate the Dendra-β-actin fusion, we cut out a *Age*I-*Xho*I fragment of Dendra from pDendra-C1 plasmid and inserted it into the respective sites of pEGFP-actin vector (Clontech). To design Dendra-fibrillarin, we swapped an *Age*I-*Xho*I fragment encoding Dendra with HcRed in pHcRed-fibrillarin plasmid[31].

Confocal microscopy. Human kidney 293T-derived Phoenix Eco cell line and human carcinoma HeLa cell line were used. Cells were transfected using Lipofectamine reagent (Invitrogen) and were tested 48 h after transfection. Leica confocal inverted microscope TCS SP2 equipped with HCX PL APO lbd.BL 63× 1.4 NA oil objective and 125 mW Ar and 1 mW HeNe lasers was used for cell imaging. The green fluorescent signal was acquired at excitation 488-nm laser line and detected at 500- to 530-nm wavelength range. The red fluorescent signal was acquired using 543-m excitation laser line and detected at 560–650 nm. Scanning was performed using 400 Hz line frequency, 512 × 512 (for fibrillarin) or 1,024 × 1,024 (for vimentin) format that corresponds to 4.9 and 2.4-μs dwell time per pixel, respectively.

To study dependence of Dendra photoconversion efficiency on intensity of activating light, we used confocal laser scanning of TALON beads with an immobilized Dendra protein sample. Activation was done by scanning of 886-μm^2 regions within beads (zoom 8, line frequency 400 Hz, format 512 × 512) with 488-nm laser of varied intensity (0.016–1.6 W/cm^2). We used a single activating scan for high intensity light, and ten activating scans for low intensity light (below 0.2 W/cm^2). Dendra red fluorescence was evaluated before and after photoconversion by scanning with 543-nm laser, and signal increase was normalized per one activating scan.

Quantification of image intensities was done with Leica LSC and ImageJ software. For activated Dendra-fibrillarin and Dendra-vimentin red signal migration from activation point P0 to adjacent point P1 an efficient diffusion coefficient D was estimated as $D = A/(4\tau_{1/2})$, where A is the area of intersection of the circle with radius P0-P1 and cell boundaries (nucleus or plasma membrane), and $\tau_{1/2}$ is the half-time of signal increase in point P1 (ref. 32). A LaserCheck (Coherent) power meter was used to measure total power of the excitation light after the microscope objective. Light power density (W/cm^2) was estimated by dividing the total power by the area of the laser-scanned or illuminated region.

Note: Supplementary information is available on the Nature Biotechnology website.

ACKNOWLEDGMENTS

We thank Robert Goldman for providing us with the EGFP-vimentin vector and Alexey V. Feofanov for help in light intensity measurements. This work was supported by grants from the European Commission FP-6 Integrated Project LSHG-CT-2003-503259 (K.A.L.), the Russian Academy of Sciences for the program Molecular and Cell Biology (S.L.) and by grants GM070358 and DA019980 from the National Institutes of Health (V.V.V.).

COMPETING INTERESTS STATEMENT

The authors declare competing financial interests (see the *Nature Biotechnology* website for details).

Published online at http://www.nature.com/naturebiotechnology/
Reprints and permissions information is available online at http://npg.nature.com/reprintsandpermissions/

1. Lippincott-Schwartz, J. & Patterson, G.H. Development and use of fluorescent protein markers in living cells. *Science* **300**, 87–91 (2003).
2. Verkhusha, V.V. & Lukyanov, K.A. The molecular properties and applications of Anthozoa fluorescent proteins and chromoproteins. *Nat. Biotechnol.* **22**, 289–296 (2004).
3. Lukyanov, K.A., Chudakov, D.M., Lukyanov, S. & Verkhusha, V.V. Photoactivatable fluorescent proteins. *Nat. Rev. Mol. Cell Biol.* **6**, 885–891 (2005).
4. Chudakov, D.M. *et al.* Kindling fluorescent proteins for precise *in vivo* photolabeling. *Nat. Biotechnol.* **21**, 191–194 (2003).
5. Patterson, G.H. & Lippincott-Schwartz, J. A photoactivatable GFP for selective photolabeling of proteins and cells. *Science* **297**, 1873–1877 (2002).
6. Ando, R., Hama, H., Yamamoto-Hino, M., Mizuno, H. & Miyawaki, A. An optical marker based on the UV-induced green-to-red photoconversion of a fluorescent protein. *Proc. Natl. Acad. Sci. USA* **99**, 12651–12656 (2002).
7. Wiedenmann, J. *et al.* EosFP, a fluorescent marker protein with UV-inducible green-to-red fluorescence conversion. *Proc. Natl. Acad. Sci. USA* **101**, 15905–15910 (2004).
8. Chudakov, D.M. *et al.* Photoswitchable cyan fluorescent protein for protein tracking. *Nat. Biotechnol.* **22**, 1435–1439 (2004).
9. Ando, R., Mizuno, H. & Miyawaki, A. Regulated fast nucleocytoplasmic shuttling observed by reversible protein highlighting. *Science* **306**, 1370–1373 (2004).
10. Verkhusha, V.V. & Sorkin, A. Conversion of the monomeric red fluorescent protein into a photoactivatable probe. *Chem. Biol.* **12**, 279–285 (2005).
11. Tsutsui, H., Karasawa, S., Shimizu, H., Nukina, N. & Miyawaki, A. Semi-rational engineering of a coral fluorescent protein into an efficient highlighter. *EMBO Rep.* **6**, 233–238 (2005).
12. Post, J.N., Lidke, K.A. & Rieger, B. Arndt-Jovin, D.J. One- and two-photon photoactivation of a paGFP-fusion protein in live *Drosophila* embryos. *FEBS Lett.* **579**, 325–330 (2005).
13. Labas, Y.A. *et al.* Diversity and evolution of the green fluorescent protein family. *Proc. Natl. Acad. Sci. USA* **99**, 4256–4261 (2002).
14. Mizuno, H. *et al.* Photo-induced peptide cleavage in the green-to-red conversion of a fluorescent protein. *Mol. Cell* **12**, 1051–1058 (2003).
15. Karasawa, S., Araki, T., Yamamoto-Hino, M. & Miyawaki, A. A green-emitting fluorescent protein from Galaxeeidae coral and its monomeric version for use in fluorescent labeling. *J. Biol. Chem.* **278**, 34167–34171 (2003).
16. Nienhaus, G.U. *et al.* Photoconvertible fluorescent protein EosFP-biophysical properties and cell biology applications. *Photochem. Photobiol.,* published online 17 August 2005 (doi:10.1562/2005-05-19-RA-533).
17. Matz, M.V. *et al.* Fluorescent proteins from nonbioluminescent Anthozoa species. *Nat. Biotechnol.* **17**, 969–973 (1999).
18. Ballestrem, C., Wehrle-Haller, B. & Imhof, B.A. Actin dynamics in living mammalian cells. *J. Cell Sci.* **111**, 1649–1658 (1998).
19. Rusan, N.M., Fagerstrom, C.J., Yvon, A.M. & Wadsworth, P. Cell cycle-dependent changes in microtubule dynamics in living cells expressing green fluorescent protein-alpha tubulin. *Mol. Biol. Cell* **12**, 971–980 (2001).
20. Yoon, M., Moir, R.D., Prahlad, V. & Goldman, R.D. Motile properties of vimentin intermediate filament networks in living cells. *J. Cell Biol.* **143**, 147–157 (1998).
21. Phair, R.D. & Misteli, T. High mobility of proteins in the mammalian cell nucleus. *Nature* **404**, 604–609 (2000).
22. Chou, Y.-H., Opal, P., Quinlan, R.A. & Goldman, R.D. The relative roles of specific N- and C-terminal phosphorylation sites in the disassembly of intermediate filament in mitotic BHK-21 cells. *J. Cell Sci.* **109**, 817–826 (1996).
23. Helfand, B.T., Chang, L. & Goldman, R.D. Intermediate filaments are dynamic and motile elements of cellular architecture. *J. Cell Sci.* **117**, 133–141 (2004).
24. Verkhusha, V.V., Chudakov, D.M., Gurskaya, N.G., Lukyanov, S. & Lukyanov, K.A. Common pathway for the red chromophore formation in fluorescent proteins and chromoproteins. *Chem. Biol.* **11**, 845–854 (2004).
25. Nienhaus, K., Nienhaus, G.U., Wiedenmann, J. & Nar, H. Structural basis for photo-induced protein cleavage and green-to-red conversion of fluorescent protein EosFP. *Proc. Natl. Acad. Sci. USA* **102**, 9156–9159 (2005).
26. He, Y.Y., Huang, J.L. & Chignell, C.F. Delayed and sustained activation of extracellular signal-regulated kinase in human keratinocytes by UVA: implications in carcinogenesis. *J. Biol. Chem.* **279**, 53867–53874 (2004).
27. Provost, N., Moreau, M., Leturque, A. & Nizard, C. Ultraviolet A radiation transiently disrupts gap junctional communication in human keratinocytes. *Am. J. Physiol. Cell Physiol.* **284**, C51–C59 (2003).
28. Ho, S.N., Hunt, H.D., Horton, R.M., Pullen, J.K. & Pease, L.R. Site-directed mutagenesis by overlap extension using the polymerase chain reaction. *Gene* **77**, 51–59 (1989).
29. Patterson, G., Day, R.N. & Piston, D. Fluorescent protein spectra. *J. Cell Sci.* **114**, 837–838 (2001).
30. Bevis, B.J. & Glick, B.S. Rapidly maturing variants of the Discosoma red fluorescent protein (DsRed). *Nat. Biotechnol.* **20**, 83–87 (2002).
31. Fradkov, A.F. *et al.* Far-red fluorescent tag for protein labelling. *Biochem. J.* **368**, 17–21 (2002).
32. Yokoe, H. & Meyer, T. Spatial dynamics of GFP-tagged proteins investigated by local fluorescence enhancement. *Nat. Biotechnol.* **14**, 1252–1256 (1996).